

: M&\$%&GhU i g'F Ydcfhcb'Gi V[ fci d'  
@VfUfm8 Yj Ycda Ybh

---

Nuclear Engineering Division

**About Argonne National Laboratory**

Argonne is a U.S. Department of Energy laboratory managed by UChicago Argonne, LLC under contract DE-AC02-06CH11357. The Laboratory's main facility is outside Chicago, at 9700 South Cass Avenue, Argonne, Illinois 60439. For information about Argonne, see [www.anl.gov](http://www.anl.gov).

**Availability of This Report**

This report is available, at no cost, at <http://www.osti.gov/bridge>. It is also available on paper to the U.S. Department of Energy and its contractors, for a processing fee, from:

U.S. Department of Energy

Office of Scientific and Technical Information

P.O. Box 62

Oak Ridge, TN 37831-0062

phone (865) 576-8401

fax (865) 576-5728

[reports@adonis.osti.gov](mailto:reports@adonis.osti.gov)

**Disclaimer**

This report was prepared as an account of work sponsored by an agency of the United States Government. Neither the United States Government nor any agency thereof, nor UChicago Argonne, LLC, nor any of their employees or officers, makes any warranty, express or implied, or assumes any legal liability or responsibility for the accuracy, completeness, or usefulness of any information, apparatus, product, or process disclosed, or represents that its use would not infringe privately owned rights. Reference herein to any specific commercial product, process, or service by trade name, trademark, manufacturer, or otherwise, does not necessarily constitute or imply its endorsement, recommendation, or favoring by the United States Government or any agency thereof. The views and opinions of document authors expressed herein do not necessarily state or reflect those of the United States Government or any agency thereof, Argonne National Laboratory, or UChicago Argonne, LLC.

**: M&\$%&Gh g'FYdcfhcb'Gi V[ fci d'@VfUfmi8 Yj Y'cda Ybh**

---

by  
M. A. Smith, C. H. Lee, and G. Yesilyurt  
Nuclear Engineering Division, Argonne National Laboratory

September 30, 2012



## SUMMARY

The goal of SHARP is to develop a suite of modern simulation tools for use on all reactor types of interest. Part of that desire is to build a heterogeneous neutron transport capability which gives accurate, detailed power distributions throughout the entire reactor core, of which we have focused our efforts on deterministic methodologies. The existing SHARP neutronics tool has demonstrated good accuracy when using conventional homogeneous modeling, but when applied on fully heterogeneous problems such as the Advanced Test Reactor (ATR) and Zero Power Reactors (ZPR), the results were not acceptable. These errors are primary attributable to the use of a three step cross section generation procedure (unit cell, lattice, and whole core). Given the success of the DeCART tool on thermal spectrum systems such as PWR, BWR, and VHTR, the subgroup methodology was identified as a potential means by which to resolve the cross section related problems in the NEAMS tools. The subgroup project in NEAMS is thus focused on creating a general purpose cross section methodology that is usable on both thermal and fast spectrum systems.

The subgroup methodology is a well studied scheme appearing very early in the nuclear engineering literature. We investigated using the subgroup methodology as a potential means to handle fast reactor problems. A considerable amount of work was performed on the subgroup library software for NEAMS where several subgroup formulations were investigated. Further, while the subgroup method has been demonstrated to be accurate enough on several problems via our own experiences with DeCART, it is not clear what its accuracy will be on more complicated problems such as the ATR.

In any case, one must have a capability to generate a library in which subgroup parameters can cover neutron spectrum characteristics of the reactor of interest. For better accuracy, we propose to use MCNP as an alternative pin-cell calculation means of generating the subgroup data and have developed a prototype code package to demonstrate the capability.

With regard to fast spectrum systems, there are numerous concerns with the subgroup methodology in which the conventional Bondarenko iteration approach often used would not accurately handle the resonance interference effect that becomes more complex and important in a fast reactor. An alternative methodology involving the local escape cross section looks promising, but substantial research needs to be completed and a basic algorithm tested before success can be confirmed.

Overall, the creation of a subgroup library application was not finished, primarily due to the fact that a bulk of the funding was moved into the next fiscal year. A better understanding of the underlying methodology was gained and a means by which to generate subgroup data was created. The work on the subgroup method for an

Application Program Interface (API) is thus not complete and can be expected to continue into the next year.

## TABLE OF CONTENTS

Summary.....	4
Table of Contents.....	6
List of Figures.....	7
List of Tables.....	7
1 Introduction.....	8
2 Subgroup Review.....	9
2.1 Solution of the Slowing Down Equation.....	9
2.2 The Subgroup Method.....	10
2.3 Modifications in DeCART.....	14
2.4 The Subgroup Solution Algorithm.....	15
3 Subgroup Software Development.....	16
3.1 Preliminary Subgroup Application Programmer Interface Design.....	17
4 Fast Reactor Application of the Subgroup Methodology.....	19
4.1 Use of MCNP for Reference Pin-Cell Calculations.....	20
4.2 Initial Thermal Reactor Tests.....	22
4.3 Fast Spectrum Methodology Development.....	22
4.4 Forward Looking Fast Spectrum Research.....	24
5 Conclusions.....	26
6 References.....	27

## LIST OF FIGURES

Figure 1. Integration Scheme for Representing a Cross Section .....	11
Figure 2. Subgroup Algorithm for Computing Microscopic/Macroscopic Data .....	17
Figure 3. Subgroup Software Outline. ....	19
Figure 4. 72-Group Absorption Cross Sections of U-238 for the VHTR Pin Cell .....	21
Figure 5. Generation Procedure for a Multigroup Subgroup Cross Section Library .....	21
Figure 6. % Difference of 72-Group Absorption Cross Sections of U-238 between DeCART and MCNP for a Typical VHTR Pin-cell .....	22
Figure 7. Convergence of the Geometry-dependent Background Cross Sections of the Fuel Region (Center) for the 3-region Cylindrical Pin Cell Problem .....	24
Figure 8. Self-shielded UFG Total Cross Sections of U-238 (Region 1) and Fe-56 (Region 2) .....	26

## LIST OF TABLES

Table 1. Specification of the Three-region Cylindrical Problem .....	25
--	----

## 1 Introduction

The goal of SHARP [1] is to develop a suite of modern simulation tools for use on all reactor types of interest. The basic goal is to reduce the uncertainties and biases in various areas of reactor design activities by providing enhanced prediction capabilities. For the fast reactor component, a high-fidelity deterministic neutron transport code named UNIC [2-3] was developed, now termed PROTEUS-SN2ND or SN2ND. The application scope of PROTEUS-SN2ND ranges from conventional homogenized assembly approaches to explicit geometry, time dependent transport calculations coupled to thermal-hydraulics and structural mechanics calculations for reactor accident simulations. The creation of a single solver that can perform all of these calculations and be competitive with the wide range of analysis tools already in use is somewhat formidable.

While PROTEUS-SN2ND has demonstrated good accuracy for homogeneous fast reactor problems [4,5] and partially heterogeneous fast reactor problems [6], when applied on fully heterogeneous problems such as the ATR [7], the results were not as exemplary. Of course it is not the solver of the transport equation itself that introduces the large errors, but the multi-group cross section data the user feeds into the solver that is [7]. The fundamental problem in generating such data arises from the equivalence that is assumed to exist between the cross section generation step (i.e. lattice calculation) and the full core heterogeneous calculation. In a conventional lattice code, the cell intended for homogenization is chosen to be periodic or repeating in the domain. In the ATR, no such repetition exists and there is no equivalent homogenization approach to conventional methodologies. However, the partially heterogeneous ZPR did involve periodic surfaces [6] and the accuracy was observed to reduce incrementally with an increasing amount of spatial heterogeneity. This error was attributed to an incorrect spectrum in the heterogeneous full core calculation with respect to the lattice calculation used to generate the cross sections. A similar cross section generation process was used for ATR which also yielded poor results .

It is from this point that we consider the DeCART [8,9] approach that is predominately used for thermal reactor systems. DeCART (and several others similar codes) merge the lattice calculation step with the whole core calculation in order to provide a full core heterogeneous solution. In general, for accurate thermal reactor calculations, one must have an accurate estimate of the continuous energy thermal spectrum to generate effective multi-group cross sections. Given that whole core continuous energy solutions are not practical, we are left with setting up a representative problem that can be used to generate the needed spectrum. DeCART relies upon the subgroup methodology [10] in which the subgroup parameters of individual isotopes are functionalized in terms of the background cross section and temperature in order to account for localized changes in spectrum due to material and geometry changes. The subgroup methodology is a well studied scheme, appearing very early in the nuclear engineering literature. The goal of the NEAMS subgroup work was to implement the subgroup methodology into solvers like PROTEUS-SN2ND. In addition,

we investigated using the subgroup methodology as a potential means to handle fast reactor problems.

## 2 Subgroup Review

The following derivation follows (paraphrases) what is described in the HELIOS methods guide [10] which is the most detailed description of the subgroup methodology found thus far. To begin, the energy variable is broken into three distinct ranges assuming the conventional multi-group methodology.

$$\Psi(\vec{r}, E, \Omega) \rightarrow \begin{pmatrix} \Psi_{g \in 1, ARR}(\vec{r}, \Omega) \\ \Psi_{g \in ARR+1, RR}(\vec{r}, \Omega) \\ \Psi_{g \in RR+1, BRR}(\vec{r}, \Omega) \end{pmatrix} \quad (2.1)$$

In this equation we see the angular neutron flux and three different ranges. ARR stands for the “Above” the Resonance Range that is in the energy range where fission neutrons are being emitted. RR stands for the Resonance Range where no fission neutrons are present (in most cases this includes a considerable portion of the unresolved resonance range). In general, RR is well above the thermal neutron range of the system. Finally, BRR is “below” the resonance range. This terminology is loosely defined and can be considered a reactor specific definition closely associated with how the slowing down equation is solved.

### 2.1 Solution of the Slowing Down Equation

Starting with the transport equation

$$\hat{\Omega} \cdot \nabla \Psi(\vec{r}, E, \hat{\Omega}) + \Sigma_t(\vec{r}, E) \Psi(\vec{r}, E, \hat{\Omega}) = S(\vec{r}, E, \hat{\Omega}), \quad (2.2)$$

we can write the typically termed slowing down equation as

$$\Sigma_t(E) \Psi(E, \hat{\Omega}) = S(E, \hat{\Omega}). \quad (2.3)$$

The typical goal of the slowing down equation is to define effective multi-group cross sections

$$\Sigma_{x,g}(\hat{\Omega}) = \frac{\int_{E_{g+1}}^{E_g} \Sigma_{x,g}(E, \hat{\Omega}) \Psi(E, \hat{\Omega}) dE}{\int_{E_{g+1}}^{E_g} \Psi(E, \hat{\Omega}) dE} \quad E_1 > E_2 > \dots > E_{G+1}, \quad (2.4)$$

where it is not uncommon to expand the cross section into spherical harmonics to eliminate the explicit angular dependence. Using a super-position principle we can define a multi-group transport equation

$$\hat{\Omega} \cdot \nabla \Psi_g(\vec{r}, \hat{\Omega}) + \Sigma_{t,g}(\vec{r}) \Psi_g(\vec{r}, \hat{\Omega}) = S_g(\vec{r}, \hat{\Omega}), \quad (2.5)$$

where  $\Sigma_{t,g}(\vec{r})$  is actually inferring a piecewise constant distribution with respect to some mesh or geometry. The solution of equation 2.5 should preserve the reaction rates at all points in space with respect to equation 2.2.

Equations 2.4 and 2.5 are in fact not valid since they are fundamentally tied to each other in that  $\Psi(E, \hat{\Omega})$  must be representative of  $\Psi_g(\vec{r}, \hat{\Omega})$  and vice versa. The trick to the subgroup method is to assume that we can construct a sufficient representation in  $\Psi(E, \hat{\Omega})$  that its inherent inaccuracy will not cause large errors in  $\Psi_g(\vec{r}, \hat{\Omega})$  and thus the reaction rates we get by solving equation 2.5. Since the solution of  $\Psi(E, \hat{\Omega})$  is highly dependent upon the geometry and mixture of materials, one should be careful in how equation 2.3 is solved. For thermal systems, experience shows that ARR and BRR can be treated with a simple scheme while RR must have a rigorous treatment to account for the geometric locations of materials and interactions between the various resonances.

The typical requirements placed upon equation 2.3 (depletion) are the generation of microscopic rather than macroscopic cross section data which redefines equation 2.4 as

$$\sigma_{x,g}(\hat{\Omega}) = \frac{\int_{E_{g+1}}^{E_g} \sigma_x(E, \hat{\Omega}) \Psi(E, \hat{\Omega}) dE}{\int_{E_{g+1}}^{E_g} \Psi(E, \hat{\Omega}) dE} \quad E_1 > E_2 > \dots > E_{G+1}. \quad (2.6)$$

To begin, the top portion of equation 2.6 is called the resonance integral (RI) and will be tabulated.

$$RI_{A,g} = \int_{E_{g+1}}^{E_g} \int \sigma_A(E, \hat{\Omega}) \Psi(E, \hat{\Omega}) dE d\Omega. \quad (2.7)$$

## 2.2 The Subgroup Method

The subgroup method was developed by observing that the flux within the energy group could be expressed as a function of the absorption cross section rather than energy.

$$\Psi(E, \hat{\Omega}) \rightarrow \phi(\sigma_{A,g}). \quad (2.8)$$

We can thus separate the total absorption cross section for a given isotope in a given energy group into the component coming from the resonances  $\hat{\sigma}_{A,g}$  and the smooth absorption  $\bar{\sigma}_{A,g}$  such that we define

$$\sigma_{A,g} = \bar{\sigma}_{A,g} + \hat{\sigma}_{A,g}. \quad (2.9)$$

Focusing on the resonance absorption, we can transform equation 2.6 into

$$\hat{\sigma}_{A,g} = \frac{\int_{E_R} \hat{\sigma}_A \hat{\phi}(\sigma_A) \frac{dE}{d\hat{\sigma}_A} d\hat{\sigma}_A}{\int_{E_R} \hat{\phi}(\hat{\sigma}_A) \frac{dE}{d\hat{\sigma}_A} d\hat{\sigma}_A}, \quad (2.10)$$

over a given resonance which we can approximate using

$$\hat{\sigma}_{A,g} = \frac{\sum_n w_{g,n} \hat{\sigma}_{A,g,n} \hat{\phi}_{g,n}}{\sum_n w_{g,n} \hat{\phi}_{g,n}}. \quad (2.11)$$

The basic idea is to break up all of the resonances within a given energy group of interest into a set of cross section levels  $\hat{\sigma}_{A,g,n}$  and weights  $w_{g,n}$  as seen in Figure 1 where the weights are chosen to produce  $\hat{\sigma}_{A,g}$ .

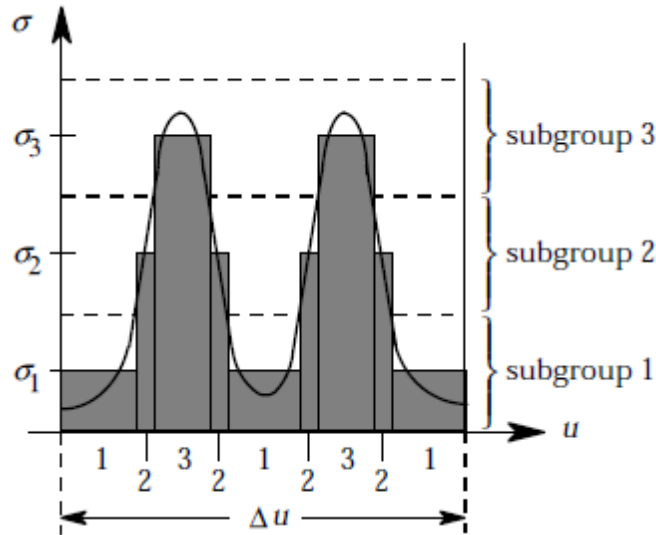


Figure 1. Integration Scheme for Representing a Cross Section

From here the derivation is a bit complicated and we skip to the conclusion that the flux solution within the resonance in the energy group can be related to the background cross section such that we can write

$$\hat{\phi}_{g,n} = \frac{\sigma_{B,g,n}}{\hat{\sigma}_{A,g,n} + \sigma_{B,g,n}}. \quad (2.12)$$

The intent of course is to use this in equation 2.11 such that we can define

$$\hat{\sigma}_{A,g} = \frac{\sum_n w_{g,n}(T) \hat{\sigma}_{A,g,n} \frac{\sigma_{B,g,n}}{\hat{\sigma}_{A,g,n} + \sigma_{B,g,n}}}{1 - \sum_n w_{g,n}(T) \frac{\sigma_{A,g,n}}{\hat{\sigma}_{A,g,n} + \sigma_{B,g,n}}}. \quad (2.13)$$

One should consult the HELIOS manual to understand the transition from equation 2.11 to 2.13, noting that the other quantities in equation 2.13 are dependent upon temperature. Of course all this is really saying is that one must now compute an appropriate background cross section. The background cross section is nice because it was observed to vary slowly within the energy group regardless of the resonances within the energy group. The background cross section in the subgroup method is computed by merging the results of  $M$  transport calculations which are created based

upon the levels  $\sigma_{g,m}$ . In DeCART, at most four levels of  $\sigma_{g,m}$  are used to represent any given energy group (as in four levels in Figure 1). The transport equation given by HELIOS is

$$\hat{\Omega} \cdot \nabla \Psi_{g,m}(\vec{r}, \hat{\Omega}) + [\Sigma_{g,m}(\vec{r}) + \lambda \Sigma_{P,g}(\vec{r})] \Psi_{g,m}(\vec{r}, \hat{\Omega}) = \lambda \Sigma_{P,g}(\vec{r}), \quad (2.14)$$

where the new terms in equation 2.12 for some mixture in the domain are defined as follows:

$$\lambda \Sigma_{P,g} = \sum_{i \in \text{isotope}} N_i \lambda \sigma_{P,g,i}, \quad (2.15)$$

$$\Sigma_{g,m} = \hat{\sigma}_{g,m} \frac{\sum_{i \in \text{isotope}} N_i RI_{A,g,i,\infty}(T)}{RI_{A,g,\text{representative},\infty}(T)}, \quad (2.16)$$

and

$$\varphi_{g,m} = \int d\Omega \Psi_{g,m}(\vec{r} \in \text{mixture}, \hat{\Omega}). \quad (2.17)$$

The basic idea is that we can compute a normalized flux quantity with respect to some source. The source in equation 2.12 is provided in the data library which is derived from the resonance scattering probability,  $\sigma_{P,g,i}$ , over the entire energy group and the distinction between a narrow or wide resonance,  $\lambda$ . It is sufficient to say that values of  $\lambda_i \sigma_{P,g,i}$  are provided in the dataset and thus pre-computed for the specific reactor type of interest and the geometry expected therein. The “representative” notation will be described later while  $RI_{g,i,\infty}(T)$  represents the resonance integral defined earlier in equation 2.7, but for each isotope in the mixture at infinite dilution. Note that it can be interpolated with respect to temperature.

Given the solutions,  $\varphi_{g,m}$ , from equation 2.17, we can construct a background cross section within each group and mixture using:

$$\Sigma_{B,g,m} = \frac{\Sigma_{g,m} \varphi_{g,m}}{1 - \varphi_{g,m}}. \quad (2.18)$$

This is of course only valid for the “representative” classification as seen in equation 2.16. We can also compute an equivalence cross section (i.e. equivalence theory cross section) as:

$$\Sigma_{E,g,m} = \Sigma_{B,g,m} - \lambda \Sigma_{P,g}. \quad (2.19)$$

We can manipulate equation 2.19 using the atom density of the isotope of interest and total mixture atom density to define an isotopic equivalence cross section

$$\sigma_{E,g,m,i} = \sigma_{B,g,m} - \lambda \sigma_{P,g,i}. \quad (2.20)$$

Similar to  $\lambda_i \sigma_{P,g,i}$ , values of  $\hat{\sigma}_{A,g,n,\text{representative}}$  are given for each isotope in each energy group for a set of  $n$  levels, but only for those isotopes designated as “representative” or  $\hat{\sigma}_{A,g,n,\text{representative}}$ . Equation 2.20 gives us  $m$  distinct values of  $\sigma_{E,g,e,m,\text{representative}}$  which are relative to the library specified values of  $\hat{\sigma}_{g,m}$ . We can assemble this into a “table” of data

from which one can interpolate the  $n$  distinct values of  $\hat{\sigma}_{A,g,n,representative}$  and thus  $\sigma_{E,g,e,n,representative}$ . Note that this is actually done using  $\ln(\hat{\sigma}_{A,g,n,representative})$  rather than  $\hat{\sigma}_{A,g,n,representative}$ . To be more explicit we can write (rep=representative)

$$\sigma_{E,g,n,rep} = \text{Interpolate} \left\{ \ln(\hat{\sigma}_{A,g,n,rep}) \text{ in } \begin{matrix} \sigma_{E,g,m=1,rep} & \ln(\hat{\sigma}_{A,g,m=1,rep}) \\ \sigma_{E,g,m=2,rep} & \ln(\hat{\sigma}_{A,g,m=2,rep}) \\ \vdots & \vdots \\ \sigma_{E,g,m=M,rep} & \ln(\hat{\sigma}_{A,g,m=M,rep}) \end{matrix} \right\}. \quad (2.21)$$

To resolve the full set of isotopic quantities, HELIOS suggests using an interpolation formula as shown in equation 2.22.

$$\hat{\sigma}_{A,g,n,i} = \left( \frac{RI_{g,representative,\infty}(T)}{RI_{g,i,\infty}(T)} \right) \hat{\sigma}_{A,g,representative,n}. \quad (2.22)$$

Rewriting equation 2.13 in terms of each isotope, we get the final relationship as shown in equation 2.23.

$$\hat{\sigma}_{A,g,i} = \frac{\sum_n w_{g,n,i}(T) \hat{\sigma}_{A,g,n,i} \frac{\sigma_{B,g,n}}{\hat{\sigma}_{A,g,n,i} + \sigma_{B,g,n}}}{1 - \sum_n w_{g,n,i}(T) \frac{\sigma_{A,g,n}}{\hat{\sigma}_{A,g,n,i} + \sigma_{B,g,n}}}, \quad (2.23)$$

where the background cross section is computed using

$$\Sigma_{B,g,n} = \Sigma_{E,g,n} + \lambda \Sigma_{P,g}. \quad (2.24)$$

This expression is of course for the "absorption" cross section and we need an additional one for the fission cross section. In that case we repeat the above methodology using a different set of levels  $\hat{\sigma}_{g,m}$  and weights  $w_{g,n,i}$ . The library actually infers separate calculations to construct non-smooth capture and fission cross section data as one would expect.

Of course equation 2.23 cannot be the final result as we must account for self shielding between different isotopes in the mixture. In DeCART a Bondarenko iterative scheme is used. To begin, the isotopic cross section data defined in equation 2.23 is only considered to be the initial estimate such that we desire the cross section:  $\Sigma_{A,g,i}^K$ . For each Bondarenko iteration we can compute the cross sections

$$\hat{\Sigma}_{A,g}^k = \sum_i N_i \hat{\sigma}_{A,g,i}^k \quad (2.25)$$

and

$$\hat{\Sigma}_{A,g,i}^k = N_i \hat{\sigma}_{A,g,i}^k. \quad (2.26)$$

For each isotope within each iteration, we compute  $\Sigma_{A,g,i}^{k+1}$  using

$$\hat{\Sigma}_{A,g,i}^{k+1} = \sum_n \frac{w_{g,n,i} \cdot \hat{\Sigma}_{A,g,n,i} \cdot \Sigma_{E,g,n,i}}{\hat{\Sigma}_{A,g,n,i} + (\hat{\Sigma}_{A,g}^k - \hat{\Sigma}_{A,g,i}^k) + \Sigma_{E,g,n,i}} \cdot \frac{1}{1 - \Delta \hat{\Sigma}_{A,g}^{k+1}} \quad (2.27)$$

Note that we also track the total change made to the absorption cross section in equation 2.26 defined as

$$\Delta \Sigma_{C,g}^{k+1} = \sum_i \sum_n \frac{w_{g,n,i} \cdot \hat{\Sigma}_{C,g,n,i}}{\hat{\Sigma}_{C,g,n,i} + (\hat{\Sigma}_{C,g}^k - \hat{\Sigma}_{C,i,g}^k) + \Sigma_{E,g,n,i}}, \quad (2.28)$$

which is initialized to zero.

Convergence of equations 2.27 and 2.28 is defined as

$$\max \left| \frac{\hat{\Sigma}_{A,g,i}^{k+1} - \hat{\Sigma}_{A,g,i}^k}{\hat{\Sigma}_{A,g,i}^{k+1}} \right| \leq 10^{-5} \quad (2.29)$$

which clearly is assumed possible in the current algorithm. Given a converged set of data in equations 2.26 and 2.27, we can calculate the macroscopic components using

$$\hat{\Sigma}_{C,g} = \sum_{isotope} \hat{\Sigma}_{A,g,i}^K > 0.0 \begin{cases} true & \hat{\Sigma}_{A,g,i}^K \\ false & 0.0 \end{cases} \quad (2.30)$$

### 2.3 Modifications in DeCART

DeCART deviates from the above HELIOS specified approach in many ways. To begin, we replace equation 2.14 with

$$\hat{\Omega} \cdot \nabla \Psi_{g,m}(\vec{r}, \hat{\Omega}) + (\Sigma_{T,g,m}(\vec{r}) - \Sigma_{PS,g}(\vec{r}) + \lambda \Sigma_{P,g}(\vec{r})) \Psi_{g,m}(\vec{r}, \hat{\Omega}) = \lambda \Sigma_{P,g}(\vec{r}), \quad (2.31)$$

where  $\Sigma_{T,g,m} = \Sigma_{g,m} + \Sigma_{PS,g} \cdot \Sigma_{ps}$  is the resonance scattering defined as

$$\Sigma_{PS,g} = \sum_i \Sigma_{PS,g,i} = \sum_i N_i \sigma_{PS,g,representative} \quad (2.32)$$

$\lambda \Sigma_{P,g}$  and  $\Sigma_{g,m}$  were defined earlier in equations 2.15 and 2.16 but are replaced with equations 2.33 and 2.34, respectively.

$$\lambda \Sigma_{P,g} = \sum_{i \in isotope} N_i \lambda \sigma_{P,g,representative}, \quad (2.33)$$

$$\Sigma_{g,m} = \frac{\sum_i N_i \cdot RI_{A,g,i,\infty}(\sqrt{T_{mesh}})}{RI_{A,g,representative,\infty}(\sqrt{T_{mesh}})} \cdot \frac{w_{g,m}(\sqrt{T_{mesh}})}{w_{g,m}(\sqrt{T_{average}})} \hat{\sigma}_{g,m} \quad (2.34)$$

Note that the usage of the weights is not consistent with the definition of  $m$  levels to build a table and the  $n$  points we desire to interpolate from that table, but there are two sets of weights provided in the data library of which both are used. In this case, we know the mesh point temperature  $T_{mesh}$  and can define an average temperature  $T_{average}$  (say temperature of fuel in a fuel assembly or core) and an average temperature in the local cell  $T_{local}$  (say over a single fuel pin).

The next major change occurs in the definition of equations 2.18 and 2.19 which uses

$$\Sigma_{E,g,m} = \begin{cases} true & -\lambda \Sigma_{P,g} + \sum_{g,m} \frac{\varphi_m}{1-\varphi_m} \\ false & 0.0 \end{cases} \quad (2.35)$$

to construct the table of data defined earlier in equations 2.20 and 2.21. Of course the interpolated quantity is also modified where we use equation 2.22

$$\hat{\sigma}_{A,g,n,i} = \frac{RI_{a,g,representative,\infty}(\sqrt{T_{local}})}{RI_{a,g,i,\infty}(\sqrt{T_{local}})} \cdot \frac{w_n(\sqrt{T_{local}})}{w_n(\sqrt{T_{average}})} \sigma_{g,n}, \quad (2.36)$$

along with the table itself

$$\sigma_{E,g,n,i} = Interpolate \left\{ \ln(\hat{\sigma}_{A,g,n,i}) \text{ in } \begin{matrix} \sigma_{E,g,m=1,rep} & \ln(\hat{\sigma}_{A,g,rep,m=1} \cdot h_{g,m=1,rep}) \\ \sigma_{E,g,m=2,rep} & \ln(\hat{\sigma}_{A,g,rep,m=2} \cdot h_{g,m=2,rep}) \\ \vdots & \vdots \\ \sigma_{E,g,m=M,rep} & \ln(\hat{\sigma}_{A,g,rep,m=M} \cdot h_{g,m=M,rep}) \end{matrix} \right\}, \quad (2.37)$$

where the new constants in the table are defined as:

$$h_{g,m,rep} = \left| \frac{w_{e,g,m}(\sqrt{T_{local}})}{w_{e,g,m}(\sqrt{T_{average}})} \right|. \quad (2.38)$$

This produces  $n$  points where the table of weights  $w_{e,g,n,local} \rightarrow w_{e,g,n}(\sqrt{T_{local}})$  and  $w_{e,g,n,average} \rightarrow w_{e,g,n}(\sqrt{T_{average}})$  are constructed simultaneously.

As one would expect, the Bondarenko iteration is also modified such that we use

$$\hat{\Sigma}_{A,g,i}^{k+1} = \sum_n \frac{w_{local,g,n,i} \cdot \hat{\Sigma}_{A,g,n,i} \cdot \Sigma_{E,g,n,i}}{\hat{\Sigma}_{A,g,n,i} \left| \frac{w_{local,g,n,i}}{w_{average,g,n,i}} \right| + (\hat{\Sigma}_{A,g}^k - \hat{\Sigma}_{A,g,i}^k) + \Sigma_{E,g,n,i}} \cdot \frac{1}{1 - \Delta \hat{\Sigma}_{A,g}^{k+1}}. \quad (2.39)$$

and

$$\Delta \Sigma_{C,g}^{k+1} = \sum_i \sum_n \frac{w_{local,g,n,i} \cdot \hat{\Sigma}_{C,g,n,i}}{\hat{\Sigma}_{C,g,n,i} \left| \frac{w_{local,g,n,i}}{w_{average,g,n,i}} \right| + (\hat{\Sigma}_{C,g}^k - \hat{\Sigma}_{C,i,g}^k) + \Sigma_{E,g,n,i}}, \quad (2.40)$$

## 2.4 The Subgroup Solution Algorithm

In the above methodology, the subgroup algorithm is a little hard to follow and requires the explanation of representative and category at this point. Given that many isotopes appearing in reactors have resonances, one can imagine that at a minimum a series of fixed source calculations should be done for each isotope if the resonances are

independent. However, the combined set of resonances actually overlap and this is accounted for in HELIOS by specifying categories within which the isotopes are lumped into resonance sets. In each resonance set, the isotopes are bunched together based upon the idea that the resonances are either not overlapped or they are overlapped, but not necessarily of equal strength (i.e. one isotope resonance dominates the overlapped resonances from a bunch of isotopes).

As an example, the first category in HELIOS assumes that all of the isotope resonances are overlapped, but that there are dominate isotopes which are termed “representative” which is obviously a subset of the full set of isotopes. All isotopes are re-indexed in terms of the representative ones as mentioned in the above formulation. The next HELIOS category separates the heavy metal isotopes (first resonance set) from the non-heavy metal isotopes (second resonance set) where again a set of representative isotopes are chosen for each resonance set. This manner continues and HELIOS is found to define nine such categories with different numbers of sets. Consistent with the first category, the last category treats each isotope independently and thus each is an individual resonance set. This would be rather expensive as outlined below and is thus rarely used.

After discussing with various DeCART users, the existing LWR and VHTR toolset is almost exclusively using the sixth category, which appears to be most accurate. This is likely consistent with the way in which the data was generated. In the sixth category, there are three resonance sets: 1) U238+Th238, 2) remaining heavy metal isotopes, 3) all non-heavy metal isotopes. For each resonance set, the representative notation above suggests that a separate set of fixed source calculations should be performed.

With this last piece of information, one can perceive a flowchart of how the subgroup methodology would be implemented which we depict in Figure 2.

### 3 Subgroup Software Development

The primary issue with using the subgroup methodology is that different applications need the cross section data for different purposes such as kinetics (or dynamics), depletion, and simple steady state solution schemes, etc. While there is a transport solver of some form used in each of these parts, it is only concerned with the resulting macroscopic quantities which is a small part compared with the needs of a depletion tool which needs microscopic quantities such as  $\sigma_{U238}(n, 2n)$ . Given that both are dependent upon the above cited data, it seems wise to store that data in a way that does not impact the performance of the transport solver (i.e. suck up usable memory). However, the fact that the subgroup methodology is quite complicated, one has to question the wisdom of multiple independent parties programming the various algorithm incarnations and dealing with the cross section data in their own ways. One specific issue is the obvious definition of a subgroup formulation of which we have shown two above and a third technically exists in DeCART for the VHTR.

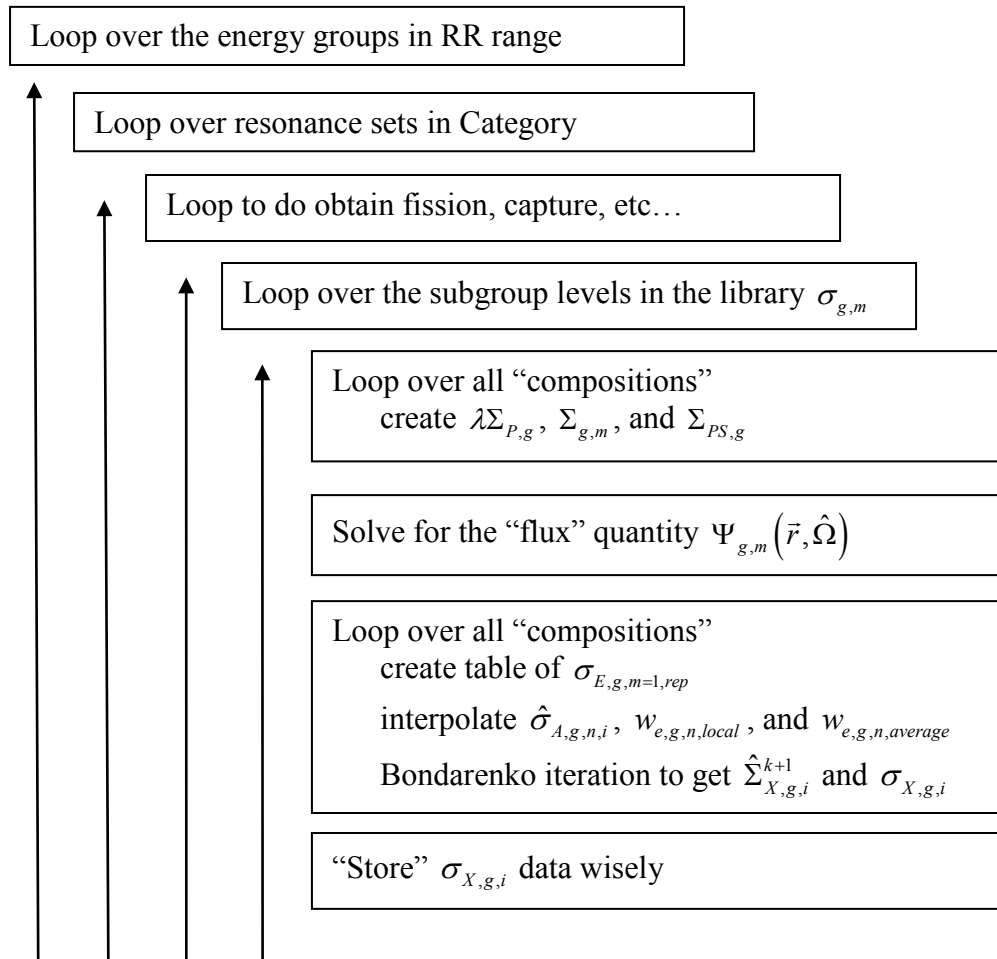


Figure 2. Subgroup Algorithm for Computing Microscopic/Macroscopic Data

### 3.1 Preliminary Subgroup Application Programmer Interface Design

The primary work on this task in the subgroup work was moved into FY13 in response to the budget reductions expected in FY13. Most of what follows is just initial planning on the subgroup Application Programmers Interface (API) noting that most of the work on the subgroup methodology was spent on a literature survey of the subgroup methodology, investigating the modifications made to it in DeCART, and researching on applications of the subgroup methodology to fast spectrum systems.

From a naïve programmer’s point of view, the subgroup algorithm can be viewed as a set of functions which require user input to produce the desired output for a targeted work scope (i.e. depletion, kinetics, etc...) with specific considerations to performance (memory usage). The output from the set of functions is identical and independent of the subgroup method itself although how it is used and maintained internal to the set of functions might be different depending upon the targeted usage (depletion, kinetics, etc...). This of course could be handled with simple input controls that specify which data is generated and how it is stored/retrieved. So in a sense, we could consider the

subgroup methodology to be a piece of software within which we can contain the mess of gibberish that is the subgroup methodology and assume the application developer understands how to interface with the software.

The input for an API begins by defining the geometry and a list of compositions made up with isotope data stored on the data file. The most general case is to assume the domain has  $E$  distinct elements with  $C$  unique compositions and a mapping between each element and its assigned composition. Because the above cited algorithm requires interpolation of temperature, we must assume at a minimum that within each element we know the temperature. Depending upon the transport solver, it may prefer to work with cross section data on a coarser grid such as the composition basis,  $C$ , or some other intermediate macro-region basis,  $R$ . The API input would thus contain:

$E$	Number of elements in the geometry
$R$	Number of macro-regions in the geometry
$C$	Number of unique compositions in the geometry
$F_T$	Flag indicating how the transport data is stored
$F_S$	Flag indicating how the data should be stored internally
$F_M$	Flag indicating how the memory should be managed internally

We must also expect that the set of functions should work with existing element-wise mapping data provided by the user such as  $\text{Composition}(E)$  and  $\text{MacroRegion}(E)$ .

One rather tricky issue to consider is how to handle the composition information. In practice, a depletion and kinetics code is going to need to know the isotopic breakdown of information while a transport solver does not. As a consequence, the individual developer would prefer that the software be able to interface with the existing data structures in each specific code rather than duplicating the detailed isotopic breakdown of each composition or requiring changes to each code. The same question arises with how the macroscopic cross section data and the microscopic data is internally managed and transferred to the connecting solver. Of course, if these data structures and the necessary functions are exposed to the user, it might not be too severe of a modification compared with the concerns of duplicating data. So in a sense, while an object orientated coding approach presents itself, it might require onerous changes to an existing transport code that will not be easy to implement.

Figure 3 shows the simplistic setup of the software where much of code functionality has not been displayed. Note that the impacts of energy (group) parallelization is not observable but it will affect the way the subgroup methodology is constructed.

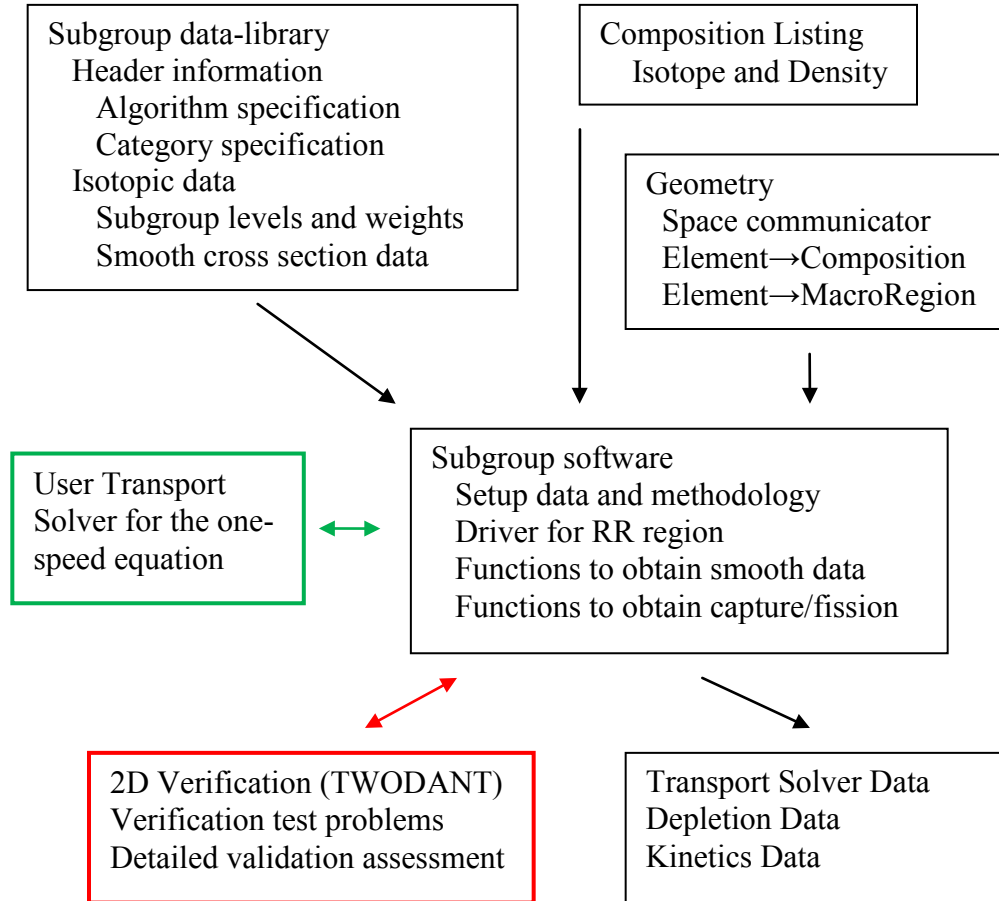


Figure 3. Subgroup Software Outline.

#### 4 Fast Reactor Application of the Subgroup Methodology

The subgroup method was originally devised for use in fast spectrum systems, but it has found its greatest use in thermal systems. This is primarily due to the fact that the treatment of the RR region is relatively insensitive to the moderator (water, graphite, molten salt, etc.). One code that does use the subgroup method is ECCO which is part of ERANOS [11]. After reviewing the literature, the subgroup formulation in ECCO is basically the same methodology as employed for the thermal systems, but it does use much more resonance groups than that observed with the thermal libraries.

A simple observation with ECCO is that it is accurate when used for compositions that are “close” to conventional fast reactor compositions with ~20% enriched fuel, but it can be considerably in error for compositions that are substantially different (~50% enriched). As a comparison point, the MC<sup>2</sup>-3 methodology [12] is more rigorous in solving the slowing down equation and does not display the same behavior. This would seem to indicate a problem with the subgroup methodology, but in reality it is just a mistake with the data library and the user. As an example, the same error growth has

been observed with DRAGON [13] and SCALE [14] when the fuel enrichment is substantially far from the typical PWR or BWR composition.

This type of behavior is consistent with the subgroup methodology because there can be multiple mixtures of materials that give the same background cross section. In such a circumstance, the component capture and fission cross sections can be erroneous because of inappropriate self-shielding which is handled during the library generation and not during the code execution. These cross section errors lead to inaccurate flux solutions in the whole core calculation, which is the reported behavior, but the fundamental issue is that the library usage is invalid and not the subgroup methodology.

To address this issue, one can understand how it can become necessary to build a cross section for specific use on a targeted reactor design (and the compositions therein). In a sense, this is equivalent to building a specific purpose multi-group library which is consistent with the modern concept of using deterministic transport methodologies to solve reactor problems rather than a stochastic one. In reality, this is already being done in the lattice codes, which use one library to target PWR and BWR, another library for VHTR, and another for fast spectrum systems, etc. To build a library, one must setup a series of representative (pin-cell) problems with correct cross sections and temperatures and solve a detailed slowing down calculation (hundreds of thousands of groups). To date, the CENTRM code from SCALE has been used to generate the subgroup library for both a PWR and VHTR system, but its methodology is not appropriate for fast spectrum systems. Further, its overall usage is problematic as it is not clear how to even model the ATR when CENTRM can only treat 1D geometries. While we can propose the use of MC<sup>2</sup>-3 as an alternative for fast spectrum systems, it is not practical to include thermal spectrum treatments at this time. Given that the various reactor designs of interest and lack of a pin-cell geometry, we researched the use of MCNP as an alternative pin-cell calculation means of generating the subgroup data.

#### **4.1 Use of MCNP for Reference Pin-Cell Calculations**

CENTRM only treats cylindrical geometries and uses the unresolved cross sections estimated from BONAMI while MCNP is obviously more flexible in terms of geometry and provides the most accurate unresolved resonance cross sections due to its continuous energy nuclear library. Figure 4 shows 72-group absorption cross sections of U-238 obtained from a VHTR pin cell calculation at 300 K using MCNP and CENTRM. As can be seen, the absorption cross section is considerably different with up to 15% error between MCNP and CENTRM. Clearly MCNP is the more accurate result and it is not necessary to state that an accurate cross section library is essential to obtaining accurate solutions in a whole-core calculation.

Since DeCART already uses the subgroup methodology and is easy to manipulate, we chose to use it as our primary test bed although this does allow us to simplify several steps in the subgroup library generation (i.e. thermal PWR and VHTR applications). The initial procedure is illustrated in Figure 5, the GenACE code produces the NJOY inputs to generate two different sets of ACE libraries for each isotope (a normal set and a set without absorption cross sections) so that only an isotope of interest in a mixture includes absorption cross sections in the MCNP calculation.

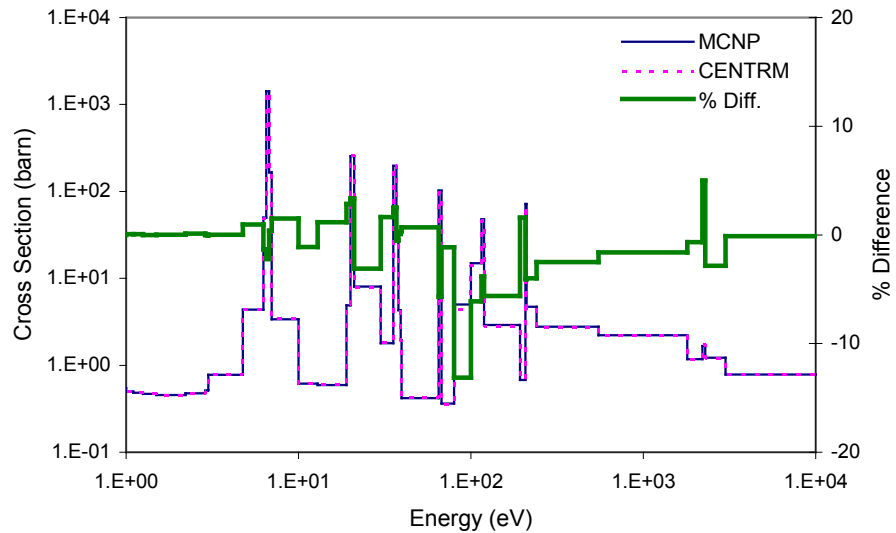


Figure 4. 72-Group Absorption Cross Sections of U-238 for the VHTR Pin Cell

The NJOY calculations are performed to produce multigroup cross sections independent of temperature and background cross section as well as the unresolved resonance cross sections as a function of temperature and background cross section. The MCNP calculations are then performed to provide the reference multigroup resonance integrals for a homogeneous mixture and a 1D pin cell geometry. Using the output from NJOY and MCNP, the GenCSL code generates the intermediate resonance parameter ( $\lambda$ ), multigroup cross section, and subgroup parameter tables for all isotopes. GenCSL solves the 1D CPM or 2D MOC fixed-source problem and does the least square fitting to determine the subgroup parameters as a function of temperature and background cross section.

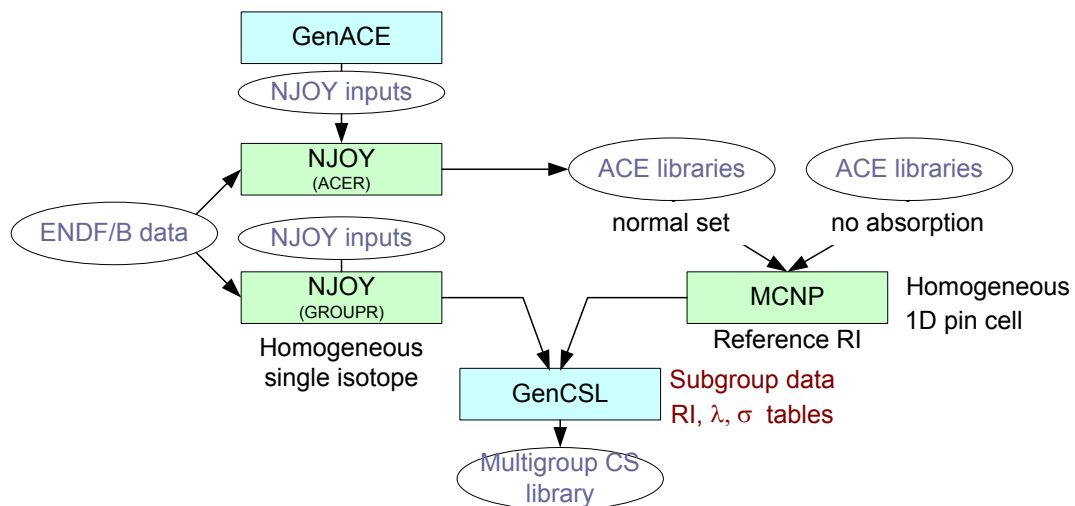


Figure 5. Generation Procedure for a Multigroup Subgroup Cross Section Library

### 4.2 Initial Thermal Reactor Tests

A full set of 72-group multi-group cross sections and parameters for U-238 only were generated, using the new system to update the existing DeCART library with the new data. DeCART was then used to run a typical VHTR pin-cell problem using the modified library. As reference solutions, a MCNP calculation was performed for the same pin-cell case (a hexagonal fuel pin with U235/U238/O/C/Si surrounded by graphite), tallying the partial cross sections of U-238 and U-235 as well as the eigenvalue.

Figure 6 shows comparison of 72-group absorption cross sections of U-238 between the old and new sets of U-238 and MCNP cross sections. Note that the old set of U-238 data was generated via the CENTRM reference solutions. In the old set of U-238, one can observe a relatively large underestimation in the absorption cross sections above 100 eV and error cancelation below 100 eV where large resonances are present at 6.7 eV and 20.8 eV. On the contrary, the new set of U-238 gives a comparatively better agreement with the MCNP cross sections than the old set.

As can be seen, there is considerably more work to be done in creating a replacement, generic purpose tool with MCNP. The preceding results do indicate that the MCNP scheme might be sufficiently suited for use in complicated thermal systems such as ATR. Follow on work will focus on extending this work to consider all isotopes and defining a standardized MCNP output interface.

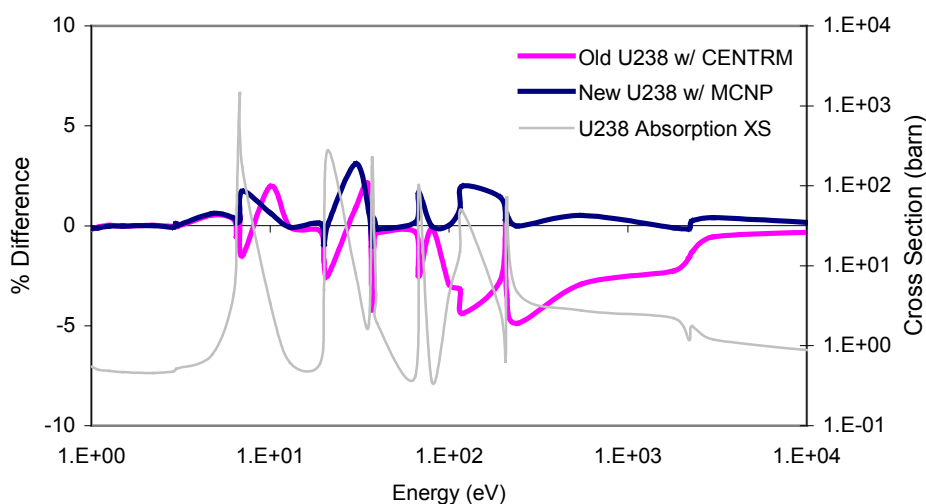


Figure 6. % Difference of 72-Group Absorption Cross Sections of U-238 between DeCART and MCNP for a Typical VHTR Pin-cell

### 4.3 Fast Spectrum Methodology Development

One of the weaknesses in the current subgroup method with respect to the fast system application is that the method relies upon the Bondarenko iteration to account for the resonance interference between different resonant isotopes. The Bondarenko iteration appears to work fine for a thermal system in which U-238 is a dominant resonant isotope, but it is not likely going to work well for fast spectrum systems that

are not dominated by U-238. The MC<sup>2</sup>-3 approach has significantly improved the accuracy of resonance self-shielding for fast spectrum systems, but it is limited to a simple 1D geometry. To account for the multi-dimensional geometry effect in resonance self-shielding, the extension of the methodology to the whole core level was considered. In this approach, the geometry-dependent background cross sections is first estimated by solving the following fixed-source transport equation in the whole-core level

$$\Omega \cdot \nabla \psi_g(r, \Omega) + \sum_{i=1}^{N_r} \left( \Sigma_{ag}^i(r) + \lambda_g^i(r) \Sigma_{pg}^i(r) \right) \psi_g(r, \Omega) = \sum_{i=1}^{N_r} \lambda_g^i(r) \Sigma_{pg}^i(r), \quad (4.1)$$

where  $\psi_g(r, \Omega)$  is the angular flux,  $N_r$  is the total number of isotopes in the region  $r$ , and  $\Sigma_{ag}(r)$ ,  $\Sigma_{pg}(r)$ , and  $\lambda_g(r)$  are the absorption and potential cross sections and the intermediate resonance parameter, respectively. The flux solution is translated to the geometry-dependent background cross section  $\Sigma_{eg}$  based on equivalence theory to get

$$\Sigma_{eg}(r) = \frac{\sum_{i=1}^{N_r} \Sigma_{ag}^i(r) \phi_g(r)}{1 - \phi_g(r)} - \sum_{i=1}^{N_r} \lambda_g^i(r) \Sigma_{pg}^i(r), \quad (4.2)$$

where  $\phi_g(r)$  is the scalar flux.

Unlike the subgroup method in which the level cross sections  $\sigma_{ng}$  are constant, the absorption cross section in the equation above should be dependent upon the resulting background cross section, and therefore a non-linear iteration is required until convergence is reached. This approach still applies the constant background cross section  $\Sigma_{eg}$  to the energy range of the group  $g$  for resonance self-shielding whose accuracy is correlated with the number of energy groups selected in the whole-core calculation. To study this behavior, MC<sup>2</sup>-3 was modified to perform the iteration between the 1D fixed-source calculation and the resonance self-shielding.

For the test problem, a cylindrical pin cell is used with three distinct regions (U235/U238/O, Cr/Ni/Fe, and Na). In the first fixed-source calculation, the infinite-dilute total cross sections are used as neutron removal from group  $g$ , while the neutron source is known with the potential scattering  $\Sigma_{pg}(r)$  for group  $g$  and region  $r$ . Once the escape cross sections are determined by the equation  $\Sigma_{eg}(r) = \Sigma_{ag}(r) \phi_g(r) / (1 - \phi_g(r)) - \Sigma_{pg}(r)$ , they are used to construct the narrow resonance flux,  $1 / (\Sigma_t(E) + \Sigma_{eg})$ , for self-shielding unresolved and resolved resonances. Those resonance cross sections are plugged again into the fixed-source equation to update the escape cross sections. Figure 7 shows the convergence behavior of the escape cross sections from the fuel region (center) of the cylindrical unit-cell problem at selected resonance groups, in which the percent differences between the current and previous escape cross sections are plotted with iteration. As can be seen, the escape cross sections converge very quickly within three iterations.

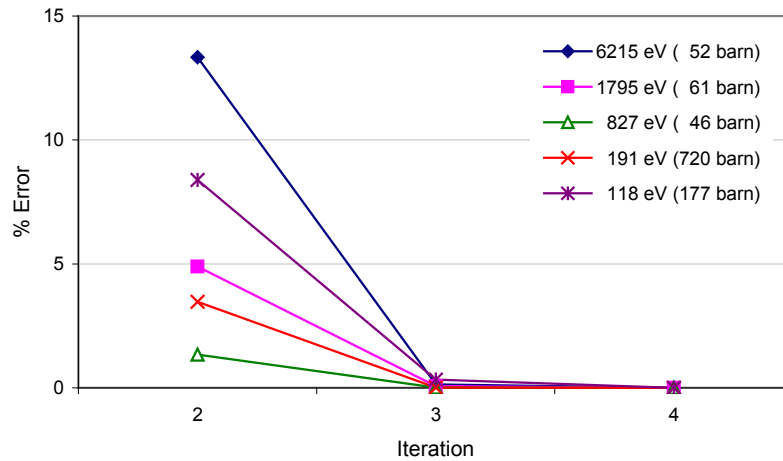


Figure 7. Convergence of the Geometry-dependent Background Cross Sections of the Fuel Region (Center) for the 3-region Cylindrical Pin Cell Problem

#### 4.4 Forward Looking Fast Spectrum Research

Due to the apparent problems with the subgroup method, the Tone's method [15] was reviewed which is based on the collision probability method. By applying the narrow resonance approximation, the flux at region  $i$  can be expressed as

$$\phi_i(E) = \frac{1}{E} \frac{\sum_j P_{ji}(E) \Sigma_{pj} V_j}{\sum_j P_{ji}(E) \Sigma_{ij}(E) V_j}, \quad (4.3)$$

where  $P_{ji}(E)$  is the collision probability from region  $j$  to  $i$ ,  $\Sigma_{ij}(E)$  and  $\Sigma_{pj}$  is the total and potential cross sections of region  $j$ , respectively, and  $V_j$  is the volume of region  $j$ . Separating out the resonant isotope  $r$  of interest, Eq. (1) can be rewritten as

$$\phi_{r,i}(E) = \frac{1}{E} \frac{\sigma_{p,r} \sum_j P_{ji}(E) N_{r,j} V_j + \sum_j \sum_{k \neq r} P_{ji}(E) \sigma_{p,k,j} V_j}{\sigma_{t,r}(E) \sum_j P_{ji}(E) N_{r,j} V_j + \sum_j \sum_{k \neq r} P_{ji}(E) \sigma_{t,k,j}(E) V_j}, \quad (4.4)$$

which can be expressed as

$$\phi_{r,i}(E) = \frac{1}{E} \frac{\sigma_{p,r} + \sigma_{p,r,i}^0(E)}{\sigma_{t,r}(E) + \sigma_{t,r,i}^0(E)}, \quad (4.5)$$

$$\text{where } \sigma_{t,r,i}^0(E) = \frac{\sum_j \sum_{k \neq r} P_{ji}(E) \Sigma_{t,k,j}(E) V_j}{\sum_j P_{ji}(E) N_{r,j} V_j}.$$

Using Tone's approximation,  $P_{ji}(E) / \Sigma_{ii}(E) = \alpha_i(E) P_{ji}^g / \Sigma_{ii}^g$ , and the additional approximation of  $\Sigma_{t,k,j}(E)$  as  $\Sigma_{t,k,j}^g$ , the background cross section above becomes a constant over group  $g$  as

$$\sigma_{t,r,i}^{0g} = \frac{\sum_j \sum_{k \neq r} P_{ji}^g \Sigma_{t,k,j} V_j}{\sum_j P_{ji}^g N_{r,j} V_j}. \quad (4.6)$$

Then, the escape cross section of the resonant isotope  $r$  at region  $i$  can be simply determined by

$$\Sigma_{t,r,i}^{eg} = N_{r,i} \sigma_{t,r,i}^{0g} - \sum_{k \neq r} \Sigma_{t,k,i}^g. \quad (4.7)$$

The escape cross section is an isotope-dependent quantity but it becomes region-dependent when the same isotope is not present at other regions. In addition, it is insensitive to the resonance interference effect. The current formulation for the escape cross section in MC<sup>2</sup>-3 has been replaced by equation 4.7.

Since equation 4.6 is based on collision probability, it is very costly to apply it for the whole core calculation. However, it is possible to solve the following two fixed source problems for the resonant isotope  $r$  as proposed by Yu [16]

$$\Omega \cdot \nabla \psi_{n,r}^g(r, \Omega) + \Sigma_t^g(r) \psi_{n,r}^g(r, \Omega) = \sum_{k \neq r} \Sigma_{tk}^g(r), \quad (4.8a)$$

$$\Omega \cdot \nabla \psi_{d,r}^g(r, \Omega) + \Sigma_t^g(r) \psi_{d,r}^g(r, \Omega) = N_r(r), \quad (4.8b)$$

which allow to estimate the background cross section in equation 4.6 without using the collision probabilities as

$$\sigma_{0,i,r}^g = \frac{\int_{V_i} dV \int_{4\pi} d\Omega \psi_{n,r}^g(r, \Omega)}{\int_{V_i} dV \int_{4\pi} d\Omega \psi_{d,r}^g(r, \Omega)} = \frac{\phi_{n,r}^g}{\phi_{d,r}^g}. \quad (4.9)$$

Using equations 4.7 through 4.8, the escape cross sections can be determined by performing  $2 \cdot N$  whole-core transport calculations where  $N$  is the number of resonant isotopes. One to two more iterations may be expected to have the total cross sections converged.

For verification, several two-region and three-region cylindrical problems were constructed with typical fast reactor compositions. In particular, a three-region problem was established based upon the simplified Monju fuel compositions and given in Table 1. Note that in this test case U-238 is present in Regions 1 and 3, while Cr-52, Fe-56, and Ni-58 are only placed in Regions 2 and 3.

Table 1. Specification of the Three-region Cylindrical Problem

Case	Composition					
	Region 1 (0.3cm)		Region 2 (0.4cm)		Region 3 (0.5cm)	
B1	U-238	1.5e-2	Cr-52	1.0e-2	U-238	1.5e-2
	U-235	4.0e-2	Fe-56	4.5e-2	Na-23	2.0e-2
	Pu-239	3.0e-5	Ni-58	7.0e-3	Cr-52	6.0e-4
	Pu-240	3.0e-3			Fe-56	2.5e-3
	O-16	1.0e-3			Ni-58	3.5e-4

The ultrafine-group (UFG) cross sections self-shielded with the escape cross sections determined by the fixed-source transport calculation (denoted by FSP) were compared

with those calculated using the 1D hyperfine-group transport calculation. Figure 8 shows the comparison between the self-shielded total cross sections with and without the escape cross sections for U-238 at Region 1 and Fe-56 at Region 2. As can be seen, the UFG cross sections self-shielded with the escape cross sections agreed well with the references. Further comparison tests will be performed with more difficult heterogeneous problems in terms of self-shielding.

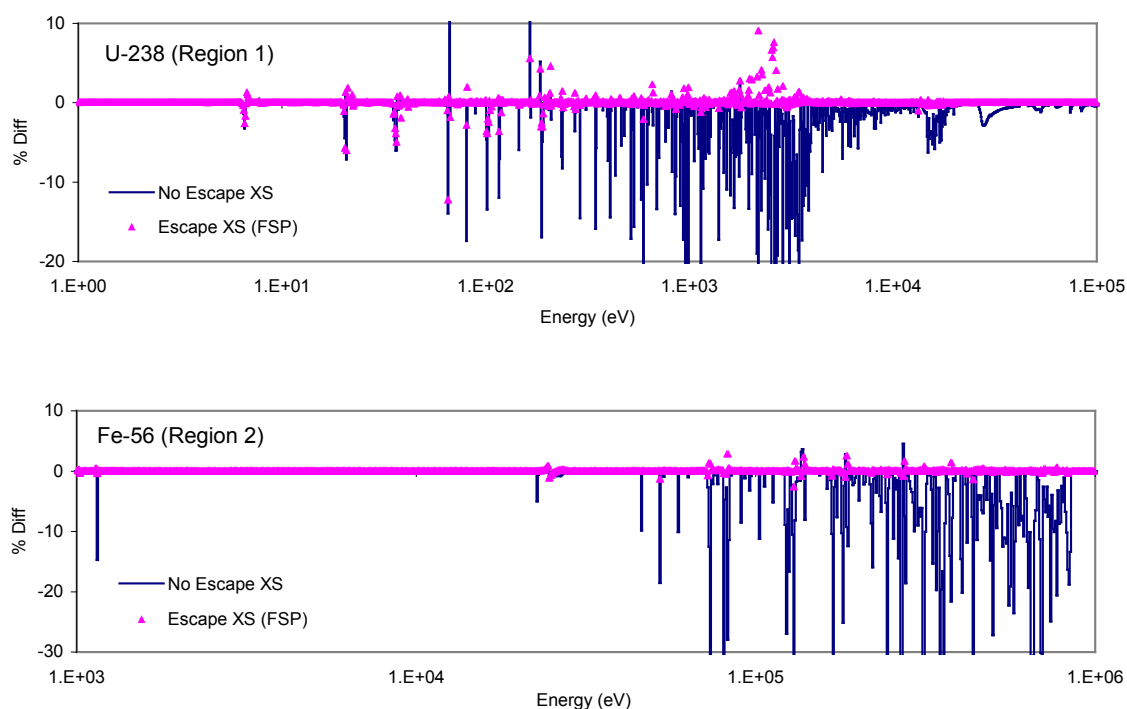


Figure 8. Self-shielded UFG Total Cross Sections of U-238 (Region 1) and Fe-56 (Region 2)

## 5 Conclusions

A considerable amount of work was performed on the subgroup library software for NEAMS. While the subgroup method has been demonstrated to be accurate enough on several problems via our own experiences with DeCART, it is not clear what its accuracy will be on more complicated problems such as ATR.

In any case, one must have a capability to generate a library in which subgroup parameters can cover neutron spectrum characteristics of the reactor of interest. For better accuracy we propose to use MCNP and have developed a prototype code package. Early demonstrations with that package indicate the inherent inaccuracy of using a deterministic slowing-down code, but MCNP is not a panacea given that the entire process is strongly based upon the “representative” geometry used to construct the library.

With regard to fast spectrum systems, there are numerous concerns with the subgroup methodology. Given the experience and background knowledge of MC<sup>2</sup>-3, we modified it to execute several scoping study tests to understand the accuracy for fast spectrum systems. As discussed, the conventional Bondarenko iteration approach often used in the subgroup methodology is not accurately handling the resonance interference effect that becomes more complex and important in a fast reactor. Additional research into the local escape cross section based methodology do look promising, but substantial research needs to be completed and a basic algorithm tested before declaring victory.

Overall, the creation of a subgroup library application was not finished, primarily due to the fact that a bulk of the funding was moved into the next fiscal year. While this did conveniently correspond with the budget troubles, the real issue is that a general purpose subgroup methodology is not apparent at this time due to the troubles encountered with the fast spectrum system. While a better understanding of the underlying methodology was gained and a means by which to generate cross section data was created, the definition of the API itself remains very vague. Consequently, any API created today would simply result in a thermal spectrum only methodology, which is not the goal of the subgroup API task in NEAMS.

## 6 References

1. A. Siegel, T. Tautges, A. Caceres, D. Kaushik, and P. Fischer, "Software Design of SHARP," *Proc. Joint Int'l Topical Mtg. on Mathematics & Computation and Supercomputing in Nuclear Applications*, Monterey, California, April 15–19 (2007).
2. M. A. Smith, A. Mohamed, A. Marin-Lafleche, E. E. Lewis, K. Derstine, C. H. Lee, A. Wollaber and W. S. Yang. FY2010 Status Report on Advanced Neutronics Modeling and Validation, ANL-GenIV-149 (September 2010).
3. M. A. Smith, D. Kaushik, A. Wollaber, W. S. Yang, B. Smith, C. Rabiti, G. Palmiotti, "Recent Research Progress on UNIC at Argonne National Laboratory," International Conference on Mathematics, Computational Methods & Reactor Physics, Saratoga Springs, New York, May 3-7 (2009).
4. M. A. Smith, A. Mohamed, A. Marin-Lafleche, E. E. Lewis, K. Derstine, C. H. Lee, A. Wollaber, and W. S. Yang, "FY2010 Status Report on Advanced Neutronics Modeling and Validation," ANL-GenIV-149 (September 2010).
5. M. A. Smith, A. Mohamed, C. H. Lee, A. Marin-Lafleche, and W. S. Yang, "Zero Power Fast Reactor Deterministic Modeling with Heterogeneous Geometry," American Nuclear Society, Hollywood, FL, June 26-30 (2011).
6. A. Mohamed, W. S. Yang, M. A. Smith, and C. H. Lee, "Spectrum Interaction Effects on Calculating Foil Reaction Rates in ZPR Assemblies," International Conference on Advances in Mathematics, Computational Methods, and Reactor Physics (M&C), Rio de Janeiro, Brazil, in May 8-12 (2011).
7. E. R. Wolters and M. A. Smith, "Scoping Analysis of the Advanced Test Reactor Using SN2ND," ANL/12-31, June (2012).
8. D.P. Weber et al, "High Fidelity LWR Analysis with the Numerical Nuclear Reactor," *Nuclear Science and Engineering*, **155**, 395-408 (2007).

9. J. Y. Cho, et al., "Whole Core Transport Calculation Employing Hexagonal Modular Ray Tracing and CMFD Formulation," *J. Nucl. Sci. Tech.*, **45**, 745-751 (2008).
10. HELIOS Methods, Studsvik Scandpower, November 20 (2003).
11. G. Rimpault, et al., "The ERANOS Code and Data System for Fast Reactor Neutronic Analyses," *Proc. of PHYSOR 2002 Conference*, Seoul, South Korea (October 2002).
12. C. H. Lee and W. S. Yang, "Development of Multigroup Cross Section Generation Code MC2-3 for Fast Reactor Analysis," International Conference on Fast Reactors and Related Fuel Cycles, Kyoto, Japan, December 7-11 (2009).
13. Marleau, G., A. Hébert, R. Roy, A User's Guide for DRAGON, Ecole Polytechnique de Montréal (December 1997).
14. SCALE: A Comprehensive Modeling and Simulation Suite for Nuclear Safety Analysis and Design, ORNL/TM-2005/39, Version 6.1, Oak Ridge National Laboratory, Oak Ridge, Tennessee, June 2011. Available from Radiation Safety Information Computational Center at Oak Ridge National Laboratory as CCC-785.
15. T. Tone, "A Numerical Study of Heterogeneity Effects in Fast Reactor Critical Assemblies," *J. Nucl. Sci. Technol.*, **12**, 467 (1975).
16. H. Yu, T. Endo, and A. Yamamoto, "Resonance Calculation for Large and Complicated Geometry Using Tone's Method by Incorporating the Method of Characteristics," *J. Nucl. Sci. Technol.*, **48**, 3, 330-336 (2011).



**Nuclear Engineering Division**

Argonne National Laboratory  
9700 South Cass Avenue, Bldg. 208  
Argonne, IL 60439

[www.anl.gov](http://www.anl.gov)



U.S. DEPARTMENT OF  
**ENERGY**

A U.S. Department of Energy laboratory  
managed by UChicago Argonne, LLC